PCCP

Monitoring Ultrafast Intramolecular Proton Transfer Processes in an Unsymmetric β-Diketone

Journal:	*Physical Chemistry Chemical Physics*
Manuscript ID:	CP-ART-12-2014-005811.R1
Article Type:	Paper
Date Submitted by the Author:	28-Jan-2015

Complete List of Authors:	Verma, Pramod; Universität Würzburg, Institut fuer Physikalische und Theoretische Chemie Steinbacher, Andreas; Universität Würzburg, Institut für Physikalische und Theoretische Chemie Koch, Federico; Universität Würzburg, Institut für Physikalische und Theoretische Chemie Nuernberger, Patrick; Ruhr-Universität Bochum, Physikalische Chemie II; Universität Würzburg, Institut fuer Physikalische und Theoretische Chemie Brixner, Tobias; Universität Würzburg, Institut für Physikalische Chemie

Phys Chem Chem Phys RSCPublishing

ARTICLE

Monitoring Ultrafast Intramolecular Proton Transfer Processes in an Unsymmetric β-Diketone

Cite this: DOI: 10.1039/x0xx00000x

Received 00th January 2012,
Accepted 00th January 2012

DOI: 10.1039/x0xx00000x

www.rsc.org/

Pramod Kumar Verma[a], Andreas Steinbacher[a], Federico Koch[a], Patrick Nuernberger[a,b], and Tobias Brixner[a,*]

We report the experimental determination of the intramolecular enol-enol tautomerization rate of an unsymmetric β-diketone, benzoylacetone, with femtosecond transient absorption in the ultraviolet. Initially, there is an equilibrium of two possible enolic structures in solution, which is disturbed upon UV excitation by exciting a disproportionate fraction of one enolic form. Comparison to symmetric β-diketones, acetylacetone and dibenzoylmethane, suggests that ground-state proton transfer gives rise to additional dynamics in benzoylacetone due to the dissimilarity of the two enolic forms. In the excited molecules, the intramolecular H-bond is initially broken, followed by photochemical processes towards rotamer structures. Our studies therefore disclose intramolecular proton transfer among electronic ground as well as excited states of benzoylacetone. Considering the importance of β-diketones as common model of enol-enol tautomerization and their resemblance to enzymatic enolates, the present study provides valuable information on the ultrafast mechanism of intramolecular proton transfer processes.

Introduction

β-Diketones ($R_1COCH_2COR_2$, Scheme 1a) are important organic reagents[1], exhibit a versatile photochemistry[2] and have resemblance to the biologically highly relevant enzymatic enolates (where low-barrier H-bonds may form)[3]. They are extensively used as chelating agents because of their unique structure[1], in commercial sunscreen products owing to ultrafast deactivation processes upon UV absorption[4], and as model systems of keto-enol tautomerization. Special attention has been attributed to the intramolecular H-bond (O-H···O) in the cis-chelated enol, as the H atom can either be shared equally by both oxygen atoms (O-H-O, Scheme 1b) or can be localized near one of them (Scheme 1c). The latter case corresponds to two minima of equal (R_1=R_2) or different (R_1≠R_2) depth in the potential energy surface of β-diketones, with a barrier between the two tautomers that has to be overcome for an intramolecular proton transfer (PT). Recently, ultrafast electron diffraction experiments revealed that in acetylacetone (AA; R_1=R_2=CH_3) the H atom is bound more strongly by one oxygen atom in the electronic ground state but is shared equally in the excited state[5, 6]. Hence, these molecules have become prototype models for a number of intramolecular PT reactions which play a critical role in various chemical, enzyme catalytic and biological processes[3, 7-10].

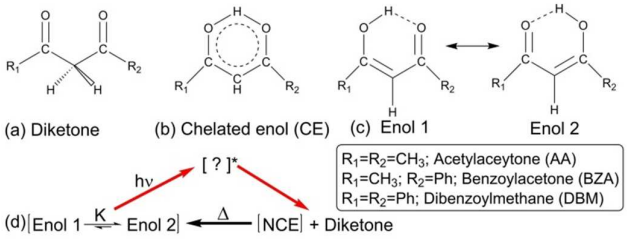

Scheme 1 Structures of different conformers of a β-diketone (a, b and c) and a simplified reaction scheme (d). The reactant, transient photoproduct (nonchelated enol, NCE) and diketone obtained on UV irradiation are known; however, the photoinduced processes upon UV excitation (red arrows) of the two tautomers (CE) in dynamic equilibrium are unknown.

In contrast to symmetric β-diketones, unsymmetric ones (R_1≠R_2) exhibit two distinguishable enolic tautomers, with the O-H either adjacent to R_1 or R_2 (Scheme 1c). In general, the two forms will differ in energy and thermodynamic stability, and the equilibrium constant *K* will not equal unity. For benzoylacetone (BZA; R_1=CH_3, R_2=Ph), Gorodetsky et al. determined a value of K = 1.29 (Enol 1 ↔ Enol 2) in aqueous solution using NMR techniques[11] suggesting that the oxygen adjacent to the phenyl ring is predominantly in the hydroxylic form (Enol 2). Hansen et al. determined[12] a value of K = 1.12 (53% of Enol 2) for BZA in CH_2Cl_2 at 227 K. This is in agreement with conclusions based on the resonance-assisted H-bond theory, proposed by Gilli et al. for a series of β-diketones[13]. A recent variable-temperature NMR study[14] of BZA in $CDCl_3$ suggested a value of 1.83 for *K*. All these results corroborate the coexistence of two enol conformers (Scheme 1c) that are in dynamic equilibrium, with more preference to Enol 2 in solution. The fate of this equilibration upon electronic excitation (Scheme 1d) is unknown and so are the subsequent relaxation dynamics.

The H atom that "belongs" to only one oxygen atom in the electronic ground state of β-diketones (confer Scheme 1) is put at the same distance from the two oxygen atoms upon vertical laser excitation (S_2←S_0)[6, 15]. This induces excited-state intramolecular proton transfer (ESIPT), taking place within approximately 70 fs for AA in the gas phase[15] whereas in solution an upper limit of 50 fs could be determined[16]. Moreover, the full dynamics are more complex than a simple ESIPT and are highly sensitive to the environment. For AA in the gas phase, the exit channel is dissociation with loss of an OH radical[6]. In contrast, when β-diketones in solution are subjected to UV irradiation, short-lived species and further products are formed[17], which fully reverse to the reactant in the dark over a period of hours[4, 17-21]. However, questions remain on the time scale of the primary processes (including the PT) leading to the formation of photoproducts in solution.

In the present study, the ultrafast dynamics after electronic excitation of an unsymmetric β-diketone with two possible enolic isomers being in dynamic equilibrium in solution (Scheme 1d) are studied and compared with symmetric β-diketones leading to identification of characteristic photoinduced processes and associated time scales. By analyzing the transient ground-state bleach, the intramolecular PT in the electronic ground state is disclosed for the unsymmetric molecule.

Results and Discussion

Spectral Characteristics

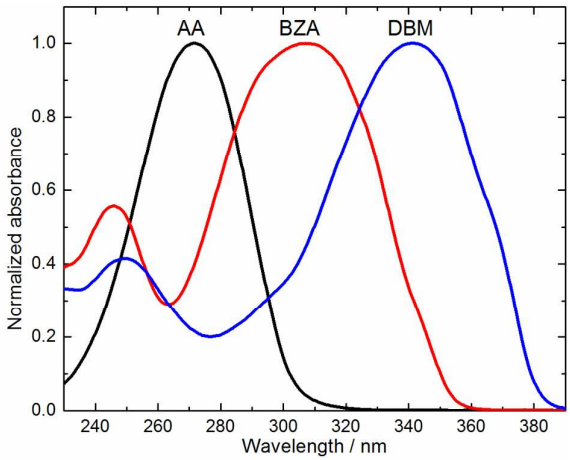

Fig. 1 Normalized absorption spectra of acetylacetone (AA), benzoylacetone (BZA) and dibenzoylmethane (DBM) in acetonitrile.

The electronic absorption bands of AA, BZA and dibenzoylmethane (DBM, R_1=R_2=Ph) lie in the UV region (Fig. 1) and are attributed to ππ* transitions (S_2←S_0) of CE species as is common for most β-diketones[17]. The minor band in the deep UV (in case of BZA and DBM) is believed to have a partial contribution from the nπ* transition of the diketone conformer (Scheme 1a)[17-19] which constitutes a small fraction of molecules in equilibrium. BZA has a large molar extinction coefficient (on the order of 10^{-4} $M^{-1}cm^{-1}$)[18] as well as a large oscillator strength[22], but fluorescence is not observed at room temperature, suggesting very efficient non-radiative deactivation processes.

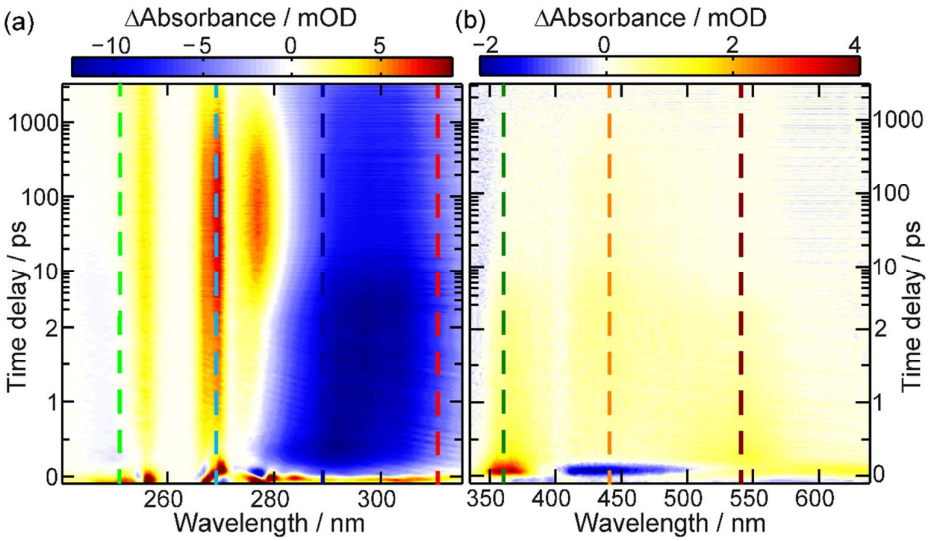

Fig. 2 TA map of BZA in acetonitrile after excitation with 335 nm (a) in the UV and (b) in the near-UV and visible regions. The "uneven" ΔAbsorbance (mOD) between 260 and 275 nm is due to the characteristic of the utilized spectral filter (see Experimental Methods). Note that the time delay is plotted on a linear scale up to 2 ps and then on a logarithmic scale. The kinetic traces at selected wavelengths (colored dashed lines) are shown in Fig. 3.

Transient Absorption

Figures 2a and b depict the transient absorption (TA) spectrum upon 335 nm excitation of BZA in acetonitrile covering the UV and the visible spectral region, respectively. The distinct negative signal (blue) in the region of 275-350 nm corresponds to the ground-state bleach (GSB). Positive signals (yellow/red) around 255-280 nm and 350-640 nm are due to induced absorption signals originating from those molecules that were excited. Furthermore, there is a sub-picosecond stimulated emission (SE) spanning from 400-500 nm (blue). Around 250-280 nm, the induced absorption signal first decays on an ultrafast time scale (100 fs), then re-rises (see below) and eventually results in a decay that remains incomplete within the experimental accessible time window of 3.3 ns. By contrast, excited-state absorption (ESA) in the 350-640 nm spectral range decays monotonously, with a negative contribution from 400-500 nm caused by the above mentioned SE.

In Fig. 3, corresponding kinetic traces at selected wavelengths are presented. At 310 and 289 nm we explicitly probe the centre and the blue edge of the GSB which show distinct dynamic behaviour up to delay times of approximately 2 ps. While a rising negative signal in the centre of the GSB region around 310 nm is detected, the dynamics at 289 nm show the opposite trend. Such differences are not observed for other symmetric β-diketones (malonaldehyde, AA and DBM)[16] and are believed to be associated with the ground state intramolecular PT (vide infra). Afterwards, in both wavelength regions, the GSB slowly recovers on a nanoseconds time scale reaching beyond our experimental time window of 3.3 ns. For a good global fit of the TA data, five time components were needed for the map of Fig. 2a (Table 1) whereas four were sufficient for the TA map of Fig. 2b (Table 1). With this approach, the time components could be determined with an accuracy of a few percent of their respective values. The corresponding evolution-associated difference spectra (EADS) are shown in Fig. S1 of Supplementary Information. Apart from the results of the measurements in acetonitrile (Figs. 2 and 3), Table 1 also contains the fitting results of TA measurements of BZA in hexane (kinetic traces at few selected wavelengths are shown in Fig. 4b and the full TA data are shown in Fig. S2 of the Supplementary Information) as well as of DBM in acetonitrile (fitting data collected from our previous study in Ref. [16]) and hexane (Fig. S3 of Supplementary Information) for comparison. A remarkable aspect of the excited-state dynamics of the unsymmetric β-diketone (BZA) is an additional positive signal in the UV region (250-280 nm) which grows in over a time of 10-100 ps (Fig. 2a and kinetic trace at 269 nm in Fig. 3) and then decays, possibly indicating a further intermediate, or structural conformer, populated in the S_1 state.

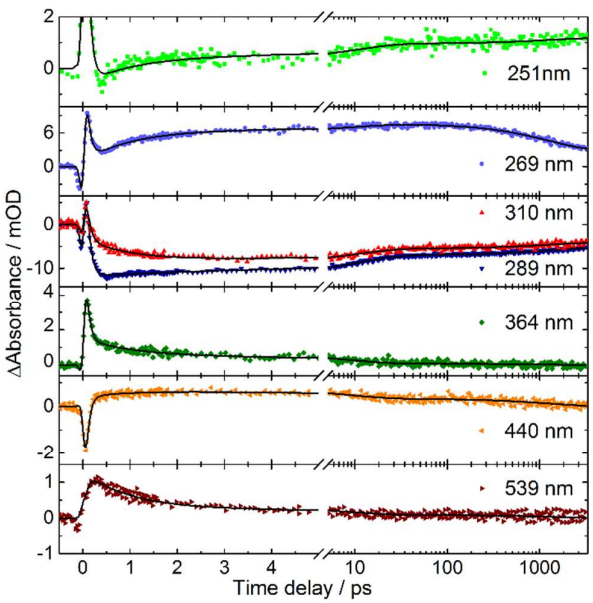

Fig. 3 Kinetic traces at selected wavelengths reflecting the ultrafast dynamics of BZA in acetonitrile. Results from the global fitting are shown in black. Note that the time delay is plotted on a linear scale up to 5 ps and then on logarithmic scale.

To check whether this intermediate is influenced by the solvent properties, additional measurements were performed in various solvents as shown in Fig. 4a, revealing that the intermediate is

influenced in a way consistent with the hydrogen-bond accepting (HBA[23]) values of the solvents, i.e., the intermediate is more pronounced with increasing HBA values. Kinetic traces at selected wavelengths in hexane and acetonitrile are juxtaposed in Fig. 4b. Whereas the evolution of excited states around 250-265 nm, 350-400 nm (see behaviour at 363 nm in Fig. 4b), and in the visible (543 nm trace in Fig. 4b) appears to be similar for the solvents, the evolution around 276 nm and 441 nm reveals additional dynamics (see Fig. 4b).

Table 1 Time components obtained by global fitting of the TA data of BZA upon 335 nm excitation and the TA data of DBM upon 340 nm excitation[16].

BZA					
TA map from Fig. 2a – deep-UV probe[c]					
solvent	τ_1 (fs)	τ_2 (ps)	τ_3 (ps)	τ_4 (ns)	τ_5[b] (ns)
acetonitrile	76	0.99	11.06	1.27	10
hexane	50[a]	0.26	8.94	-	10
TA map from Fig. 2b – near-UV / VIS probe[c]					
solvent	τ'_1 (fs)	τ'_2 (ps)	τ'_3 (ps)	τ'_4 (ns)	-
acetonitrile	67	0.97	9.29	1.28	-
hexane	50[a]	0.34	4.12	10[b]	-
DBM					
deep-UV probe[c]					
solvent	τ_1 (fs)	τ_2 (ps)	τ_3 (ps)	τ_4 (ns)	τ_5[b] (ns)
acetonitrile	147	1.18	10.75	0.49	10
hexane	50[a]	1.29	9.91	0.47	10
near-UV / VIS probe[c]					
solvent	τ'_1 (fs)	τ'_2 (ps)	τ'_3 (ps)	τ'_4 (ns)	-
acetonitrile	128	0.37	16.34	10[b]	-
hexane	98	0.33	9.61	10[b]	-

[a]The 50 fs component is an upper limit that is below the instrumental time resolution. [b]This time component corresponds to one that was fixed to 10 ns during the global fitting due to presence of an offset in the transient map. [c]The spectral ranges employed for fitting of the TA map of DBM in the deep-UV probe and near-UV / VIS probe regions are 225-322 nm and 340-640 nm, respectively.

Discussion

Excited-State Dynamics

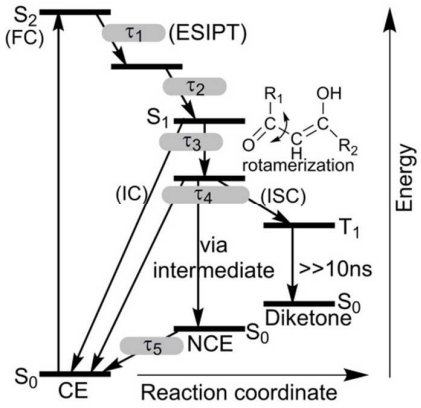

Scheme 2. An illustrative energy diagram connecting the key steps of the photoinduced processes of a β-diketone upon electronic excitation.

The vertical electronic excitation of BZA initially populates the first bright state S_2 (dipole-allowed ππ* transition), leading to an ultrafast departure from the Franck–Condon (FC) region and ESIPT in the S_2 state (confer Scheme 2). This is observable as a decaying ESA signal (see kinetic traces at 269 and 364 nm in Fig. 3 and Scheme 2) with a time constant of ≈ 70 fs (τ_1 and τ'_1 of Table 1). In smaller diketones, the ESIPT proceeds faster, < 50 fs for AA[16], while for larger β-diketones like DBM[16] and DMADK (N,N-dimethylanilino-1,3-diketone)[24] it takes place on a time scale of ≈ 150 fs. Similar photoinduced ESIPT processes have also been reported to explain the ultrafast deactivation of o-hydroxybenzaldehyde, oxybenzone, 3-hydroxypicolinic acid, and salicylic acid upon UV irradiation. Each of them exhibits an H atom donor (a hydroxyl group) and an acceptor (the carbonyl oxygen atom) in close proximity[25, 26].

Subsequently, the system moves to a region of vibronic coupling between the S_2 (ππ*) and S_1 (nπ*) surfaces where population transfer takes ≈ 1 ps for BZA in acetonitrile (τ_2 and τ'_2 of Table 1). Note that the decay constant τ_2 of Table 1 may reflect contributions from multiple processes like population transfer from S_2 to S_1, an intermediate formation in S_1 state, and re-equilibration of the enol-enol tautomerization (vide infra). However, the EADS (Supplementary Information Fig. S1) corresponding to this time component suggest that mainly enol-enol tautomerization and the intermediate formation take place. For AA (value taken from our previous measurement[16]) and DBM (Table 1) in acetonitrile, the population transfer is achieved in 2.13 ps and 1.18 ps, respectively. The difference between symmetric AA and unsymmetric BZA is that one methyl group in AA is replaced by an electron-rich phenyl group that decreases the energy gap between S_2 and S_1 states[22]. Replacing both methyl groups of AA with phenyl groups yields DBM for which the S_2–S_1 energy gap is lowered further[22].

From S_1 the relaxation can follow two non-radiative paths as sketched in Scheme 2 (radiative paths are ruled out due to the absence of fluorescence at room temperature), i.e., either internal conversion (IC) to the ground state or rotamerization. Both processes are associated with τ_3 (≈ 10 ps). The direct IC to the ground state is evident from the partial GSB recovery at early delay times (see kinetic trace at 289 and 310 nm in Fig. 3). The rotamerization in S_1 must occur prior to the photoproduct (i.e., NCE) formation or intersystem crossing[19, 21] (ISC). Most likely it occurs around the CO-CH and/or around the C=C bond where the intramolecular H-bond is almost broken as evidenced from computational and experimental studies for β-diketones[19, 20, 27, 28]. The evolution of excited states (except ISC) discussed above is in full analogy to the recent study of smaller β-diketones disclosing that after the initial PT process population transfer occurs from S_2 to S_1[16]. Then, there is a bifurcation on S_1 so that excited molecules partly undergo IC to S_0 while others undergo rotamerization on a time scale of ≈ 10 ps, followed by formation of the nonchelated enol (NCE) photoproduct on hundreds of picoseconds[16]. In addition, the bigger β-diketones (BZA and DBM having one or two phenyl groups as substituent) also exhibit ISC from the singlet to a triplet state that absorbs in the visible region (see kinetic trace at 441 nm in Figure 4b). This ISC is believed to be responsible for the formation of the Diketone form (See Schemes 1a,d and 2) and irreversible photodegradation on exposure to UV radiation[17, 21].

In case of BZA, photoproduct absorption is seen as residual positive absorbance in the 250-280 nm region at long delay times. This wavelength region corresponds well with the absorption maximum (around 265 nm) of the NCE photoproduct formed on UV irradiation as observed in flash photolysis experiments[17, 18]. The kinetic trace at 251 nm (Fig. 3) reveals a growing positive signal on a hundreds of picoseconds time scale which corroborates the NCE photoproduct

formation, whereas no such feature is present at 364 nm (where the photoproduct does not absorb). Thus, τ_4 can be related to depopulation of the S_1 state from where relaxation towards the NCE photoproduct occurs (this time component also appears to be connected to the decay of the intermediate, vide infra). In the case of hexane, such a decay component could not be assigned. This is most likely due to the lesser photoproduct absorption

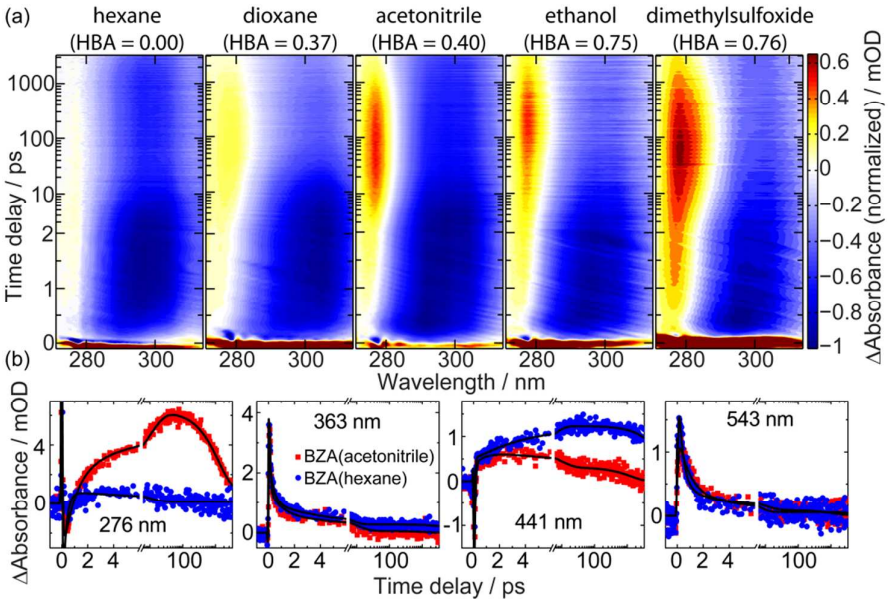

Fig. 4 TA data of BZA in different solvents. (a) The dependence of an intermediate formation is monitored in five different solvents. The positive ΔAbsorbance around 275 nm in the TA map of BZA follows the displayed HBA values (taken from Ref. 23) of the respective solvents. Each TA map data is normalized to the maximum bleach signal. (b) Kinetic traces are shown for the solvents hexane (blue) and acetonitrile (red) at selected wavelengths. Fit results from the global fitting are shown in black. Note that the abscissa is plotted on a linear scale up to 2 ps in (a) and up to 6 ps in (b), then on a logarithmic scale.

signal of BZA in hexane compared to acetonitrile in the accessible time window of 3.3 ns. Similar solvent-dependent behaviour was observed for AA where photoproduct formation in hexane was reduced to less than half of that in acetonitrile on UV excitation[16]. Once the NCE conformers are formed, they revert rather slowly to the most stable CE form[17, 18]. The fifth fixed time component (fixed to 10 ns during global fitting of the TA data in Table 1) is attributed to this slow recovery proceeding on a time scale which differs by multiple orders of magnitude from the initial dynamics observed here[17].

The intermediate absorption signal observed for BZA, as visualized in Fig. 4, merits further discussion. One putative origin is the modification of the excited-state potential energy surface (PES) of one tautomer with respect to the other in different solvents, especially if they are strong hydrogen-bond acceptors. There are two enols with slightly different energy in the ground state, and thus there will be two in the excited state with slightly different energy. On the one hand, in the nonpolar solvent hexane, photoexcitation of a mixture of Enol 1 and Enol 2 to S_2 is followed by population transfer to S_1 of two distinguishable tautomers prior to their respective decays as discussed earlier via three different channels, IC to S_0 (as seen in decay kinetics of GSB), ISC (see triplet absorption in the visible region[20], shown in the kinetic trace at 441 nm in Fig. 4b), and formation of the NCE photoproduct. On the other hand, a solvent like dioxane (dielectric constant similar to hexane) which is an H-bond acceptor (HBA = 0.37) can provide additional stabilization to the enol species in the excited state (where the intramolecular H-bond is partially broken), possibly to one isomer preferably more than to the other, and subsequent excited-state dynamics are governed by this effect. The stabilization may give rise to the absorption signal (termed as "intermediate" in Scheme 2) which is also seen in other H-bond accepting and polar solvents, most prominent in DMSO having the highest HBA (= 0.76)[23] and dielectric constant (= 47)[23] among the studied solvents (see the positive signal near 275 nm in Fig. 4a). The appearance of this intermediate absorption (e.g., in acetonitrile, see kinetic trace at 276 nm in Figure 4b) is accompanied by a reduction of the competing ISC reaction channel which is more pronounced in apolar solvents (e.g., in hexane, see triplet absorption at 441 nm in Fig. 4b), although the ground state absorption of BZA in hexane and acetonitrile do not differ significantly with absorption maxima at 306 and 307 nm, respectively. Solvent-induced modification of the PES and related consequences on the excited-state evolution have also been reported for a donor-substituted unsymmetric β-diketone, DMADK[24]. By contrast, for the symmetric β-diketone DBM we observe that the dynamics in both hexane and acetonitrile behave similarly (Table 1).

A second putative origin for the intermediate absorption in Fig. 4a is the formation of a precursor to the NCE photoproduct where the OH group and the phenyl ring transiently interact in an H-bond-like manner (as for instance surmised by Markov et al.[29]) which might not be the case in the final NCE photoproducts anymore. The solvent could play a mediating role which seems to roughly follow the H-bond accepting properties of the solvent (see HBA values[23] in Fig. 4a). However, this interaction with the phenyl ring would not explain why the effect is very pronounced in BZA but not in DBM. These aspects would be an interesting topic for future elucidation in theoretical studies.

Ground-State Dynamics

A closer look at the GSB region of BZA in acetonitrile (Fig. 5a) reveals that initially there is a higher negative signal at the lower wavelength region of GSB (below 292 nm) that over a time of approximately 2 ps shifts towards the higher wavelength region of GSB (see the arrows in Fig. 5a). During the same time interval, an isosbestic point appears near 293 nm suggesting the presence of two distinct species in equilibrium in solution.

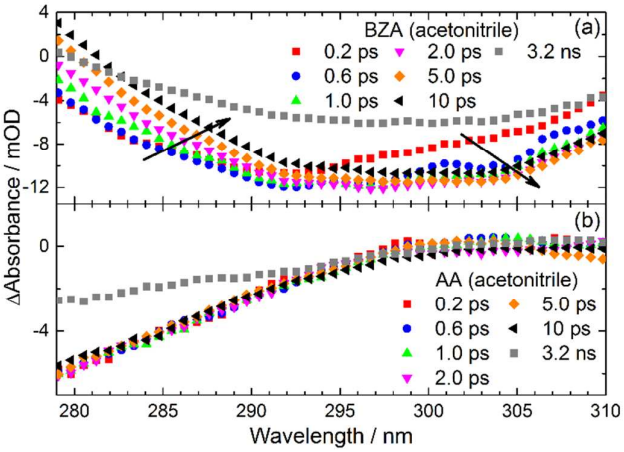

Fig. 5 Time-resolved absorbance difference spectra of (a) BZA in acetonitrile at different delay times and (b) AA (excitation wavelength = 265 nm). The spectral probe region is chosen so that no contributions from ESA or the filter used in the probe continuum generation dominate, but rather GSB signals.

In principle, a growing ESA at the blue edge of the GSB region together with a decaying one at the red edge of the GSB with an identical rise/decay constant could lead to such behaviour. However, the shift is observed for BZA in almost all of the studied solvents, but in case of hexane as the solvent, the time constants (rising and decaying ESA) have significantly different values. Hence, the shift in the GSB region, as indicated in Fig. 5a, cannot originate only from the dynamics of ESA signals at the red and blue edge of the GSB.

Besides analysing the observed dynamics in the GSB of BZA for different solvents, we also compare the behaviour to the corresponding GSB signals in symmetric β-diketones (malonaldehyde, AA and DBM). In Fig. 5b, the red edge of the GSB region of AA is displayed, which directly shows that the initial dynamics of AA are not connected to any noticeable change of the GSB spectral shape, but rather the GSB stays constant during the first 10 ps and then decays monotonously in our experimental time window. The same is true for malonaldehyde (R_1=R_2=H)[16], and also the inspection of the blue and red edge of the GSB region of DBM (as seen in the two TA maps of Fig. S3 of Supplementary Information and the corresponding time constants in Table 1) reveals a lack of pronounced dynamics in the GSB region similar to those observed for BZA. Thus, we conclude that the changes observed for BZA (Fig. 5a) are a consequence of the dynamic equilibrium of two distinguishable enolic tautomers (Enol 1 and Enol 2) in the electronic ground state compared to only one enol form possible in case of symmetric β-diketones. Recent NMR studies on BZA reported that 65% of enolization occurs in the phenyl side (Enol 2)[14]. The slightly higher stability of Enol 2 was assigned to extended conjugation between the phenyl ring and C=CH–C=O as compared with the cross conjugation present in Enol 1 (where the phenyl group is conjugated only to the C=O bond)[30].

Though the absorption spectrum of BZA has contributions from both the tautomers being in dynamic equilibrium, it cannot be deconvoluted into two separate ones since the individual contributions are not known. Upon electronic excitation, this dynamic equilibrium will be perturbed if the ratio of excited Enol 1 and excited Enol 2 does not match the equilibrium distribution. Hence, the molecules remaining in the ground state are no longer in equilibrium, so that the perpetually occurring intramolecular PT will lead to re-equilibration. Once the dynamic equilibrium is quickly re-established by intramolecular PT, the overall GSB band decays monotonously over time. An approximate estimate of this PT process in the electronic ground state is τ_2 (confer Table 1 and Scheme 2). The EADS corresponding to τ_2 (Fig. S1a in Supporting Information) is manifested in a substantial shift and increase in bleach signal compared to the EADS for τ_3. In nonpolar solvents like hexane where the solvent reorganization energy is negligible, the intramolecular PT both in the ground state (τ_2 = 0.26 ps, Table 1) and the excited state (upper limit of τ_1 = 50 fs, Table 1) becomes much faster compared to acetonitrile.

The fast intramolecular PT in the electronic ground state of diketones was recently addressed in an NMR study[31] which concluded for DBM in CCl_4 that there is basically no barrier for the intramolecular PT, while for a γ-diketone (fulvene) the intramolecular PT rate between electronic ground states was reported to be more than two orders of magnitude lower than the values reported here for BZA. For unsymmetric β-diketones like BZA, two-dimensional infrared spectroscopy[32-37] is a powerful technique sensitive to chemical exchange (e.g., hydrogen bonding), because the frequency of the carbonyl stretch vibration of the two enolic forms differ. Park and Ji recently demonstrated this for 2-acetylcyclopentanone in CCl_4 and found intramolecular PT to occur with time constants of 3.2 and 3.8 ps for going from the more stable to the other enolic form or vice versa, respectively[38], which is a timescale similar to the one of the dynamics observed here for BZA. Further insight might be accessible by 2D spectroscopy techniques for both ground- and excited-state exchange processes[32-34, 39] or by extending the UV transient absorption experiments presented here to 2D UV experiments[40-44].

Experimental Methods

BZA (CAS No. 93-91-4) and DBM (CAS No. 120-46-7) were obtained from Merck Millipore and used as received. The spectroscopic-grade solvents were obtained from Sigma-Aldrich. The steady-state absorption spectra were recorded on a Jasco V670 UV–VIS spectrophotometer. For the transient absorption measurements all samples were prepared to have an absorbance of roughly 0.3 OD in the flow cell (sample thickness 200 μm) at the excitation wavelength.

The experimental setup has been described elsewhere[16]. Briefly, pulses from a commercial Ti:sapphire regenerative-amplifier laser system (Spitfire Pro, Spectra-Physics, center wavelength 800 nm, 120 fs duration, 1 kHz repetition rate) were used to seed a non-collinear optical parametric amplifier (TOPAS White, Light Conversion Ltd.) and to generate 267 nm pulses. The visible TOPAS output was frequency doubled in a 65-μm β-barium borate crystal to generate UV pump pulses.

Approximately, 300 µW of the 267 nm beam was focused into a linearly moving 5 mm thick CaF_2 plate to generate a UV white-light supercontinuum probe ranging from 220 to 330 nm. When visible continuum was required, the fundamental 800 nm beam, rather than the third harmonic, of the amplifier system was focused into CaF_2. This was achieved by removing BBO crystals inside the THG box and replacing some of the mirrors with 800 nm high reflector mirrors. We used a custom-designed spectral filter (Laser Components GmbH) to suppress the high spectral power of the 267 nm beam contained within the UV supercontinuum probe. The pump and probe pulses were focused in non-collinear geometry and spatially overlapped in the flow cell under magic-angle configuration of pump and probe polarization to exclude contributions from rotational diffusion[45-47]. After passing the sample, the probe pulses were spectrally dispersed and detected via a spectrograph (Acton SP2500i) equipped with a CCD camera (Princeton Instruments Pixis 2k). A mechanical chopper working at 500 Hz blocked every other pump pulse, and consecutive probe signals, with a constant background subtracted, were processed on a shot-to-shot basis to obtain the pump-induced change in the absorbance of the sample. Data analysis of the transient map consisting of a three-dimensional dataset (wavelength, pump–probe delay, and absorbance change) was performed with the global analysis program Glotaran which is a graphical user interface (GUI) for the statistical computations package TIMP (scripted in R)[48-50]. Glotaran accounts for instrument response function, dispersion and coherent artifact during the fitting process. The transient absorption data were also taken with the neat solvents only. Pump-induced signals arising purely from the solvents were found to be negligible when compared to signals from β-diketones.

Conclusion

In summary, we performed a comparison of the ultrafast photochemistry of symmetric (AA, DBM) and an unsymmetric (BZA) β-diketone that share a common chelate ring. Similarities comprise an ultrafast ESIPT on a time scale of about 100 fs, followed by population transfer from the initially bright state (S_2, ππ*) to a dark state (S_1, nπ*) within a few ps, from where both nonradiative transitions to the reactants and the formation of non-chelated rotamers on a hundreds-of-picoseconds time scale are possible. In addition, intersystem crossing can take place, with the triplet state decaying faster in polar than in nonpolar solvents. For the unsymmetric β-diketone BZA, an additional excited-state intermediate species was observed and the intramolecular proton transfer corresponding to enol–enol tautomerization in the electronic ground state has been identified, which occurs on a sub-ps time scale. Our approach therefore allowed the observation of proton transfer reactions both in the electronic ground and excited state simultaneously within the same experiment.

Acknowledgements

We thank the German Research Foundation (DFG) for funding within the Research Unit "Light-Induced Dynamics in Molecular Aggregates" (FOR 1809) as well as for support of PN within the Emmy-Noether program and the Cluster of Excellence RESOLV (EXC1069). We are grateful to Dr. Ulrike Selig-Parthey, Michael Förster, and Dr. Martin Kullmann for the contribution to the UV supercontinuum generation. A.S. thanks the German National Academic Foundation (Studienstiftung des deutschen Volkes) for a scholarship.

Notes and References

Corresponding author: *brixner@phys-chemie.uni-wuerzburg.de

[a]Institut für Physikalische und Theoretische Chemie, Universität Würzburg, Am Hubland, 97074 Würzburg, Germany.

[b]Physikalische Chemie II, Ruhr-Universität Bochum, Universitätsstraße 150, 44780 Bochum, Germany.

† The authors declare no competing financial interests.

Electronic Supplementary Information (ESI) available: Evolution-associated difference spectra (EADS), transient absorption data of BZA and DBM in hexane in the UV and the VIS region. See DOI: 10.1039/b000000x/

1. R. H. Holm and F. A. Cotton, *J. Am. Chem. Soc.*, 1958, **80**, 5658-5663.
2. P. Markov, *Chem. Soc. Rev.*, 1984, **13**, 69-96.
3. B. Schiøtt, B. B. Iversen, G. K. H. Madsen, F. K. Larsen and T. C. Bruice, *Proc. Natl. Acad. Sci. U.S.A.*, 1998, **95**, 12799-12802.
4. A. Cantrell and D. J. McGarvey, *J. Photochem. Photobiol. B*, 2001, **64**, 117-122.
5. R. Srinivasan, J. S. Feenstra, S. T. Park, S. Xu and A. H. Zewail, *J. Am. Chem. Soc.*, 2004, **126**, 2266-2267.
6. S. Xu, S. T. Park, J. S. Feenstra, R. Srinivasan and A. H. Zewail, *J. Phys. Chem. A*, 2004, **108**, 6650-6655.
7. S. J. Formosinho and L. G. Arnaut, *J. Photochem. Photobiol. A*, 1993, **75**, 21-48.
8. C. L. Perrin and J. B. Nielson, *Annu. Rev. Phys. Chem.*, 1997, **48**, 511-544.
9. A. Douhal, F. Lahmani and A. H. Zewail, *Chem. Phys.*, 1996, **207**, 477-498.
10. H. J. Heller and H. R. Blattmann, *Pure Appl. Chem.*, 1973, **36**, 141-162.
11. M. Gorodetsky, Z. Luz and Y. Mazur, *J. Am. Chem. Soc.*, 1967, **89**, 1183-1189.
12. E. V. Borisov, E. V. Skorodumov, V. M. Pachevskaya and P. E. Hansen, *Magn. Reson. Chem.*, 2005, **43**, 992-998.
13. V. Bertolasi, P. Gilli, V. Ferretti and G. Gilli, *J. Am. Chem. Soc.*, 1991, **113**, 4917-4925.
14. H. Matsuzawa, T. Nakagaki and M. Iwahashi, *J. Oleo Sci.*, 2007, **56**, 653-658.
15. L. Poisson, P. Roubin, S. Coussan, B. Soep and J.-M. Mestdagh, *J. Am. Chem. Soc.*, 2008, **130**, 2974-2983.
16. P. K. Verma, F. Koch, A. Steinbacher, P. Nuernberger and T. Brixner, *J. Am. Chem. Soc.*, 2014, **136**, 14981–14989.
17. D. Veierov, T. Bercovici, E. Fischer, Y. Mazur and A. Yogev, *J. Am. Chem. Soc.*, 1977, **99**, 2723-2729.
18. D. Veierov, T. Bercovici, E. Fisher, Y. Mazur and A. Yogev, *J. Am. Chem. Soc.*, 1973, **95**, 8173-8175.
19. S. Tobita, J. Ohba, K. Nakagawa and H. Shizuka, *J. Photochem. Photobiol. A*, 1995, **92**, 61-67.
20. A. Kobayashi, M. Yamaji, S. Nakajima, K. Akiyama, S. Tero-Kubota, S.-i. Kato and Y. Nakamura, *Chem. Phys. Lett.*, 2013, **555**, 101-105.

21. A. Aspée, C. Aliaga and J. C. Scaiano, *Photochem. Photobiol.*, 2007, **83**, 481–485.
22. H. Morita and H. Nakanishi, *Bull. Chem. Soc. Jpn.*, 1981, **54**, 378-386.
23. C. Reichardt and T. Welton, *Solvents and Solvent Effects in Organic Chemistry*, Wiley, 2011, p. 471.
24. R. Ghosh and D. K. Palit, *Photochem. Photobiol. Sci.*, 2013, **12**, 987-995.
25. S. Lochbrunner, T. Schultz, M. Schmitt, J. P. Shaffer, M. Z. Zgierski and A. Stolow, *J. Chem. Phys.*, 2001, **114**, 2519-2522.
26. T. N. V. Karsili, B. Marchetti, M. N. R. Ashfold and W. Domcke, *J. Phys. Chem. A*, 2014, **10.1021/jp507282d**.
27. H. P. Upadhyaya, A. Kumar and P. D. Naik, *J. Chem. Phys.*, 2003, **118**, 2590-2598.
28. P. Roubin, T. Chiavassa, P. Verlaque, L. Pizzala and H. Bodot, *Chem. Phys. Lett.*, 1990, **175**, 655-659.
29. P. Markov and I. Petkov, *Tetrahedron*, 1977, **33**, 1013-1015.
30. S. F. Tayyari, J. S. Emampour, M. Vakili, A. R. Nekoei, H. Eshghi, S. Salemi and M. Hassanpour, *J. Mol. Struct.*, 2006, **794**, 204-214.
31. Y. Masuda, T. Nakano and M. Sugiyama, *J. Phys. Chem. A*, 2012, **116**, 4485-4494.
32. P. Hamm and M. Zanni, *Concepts and Methods of 2D Infrared Spectroscopy*, Cambridge University Press, 2011.
33. P. Hamm, J. Helbing and J. Bredenbeck, *Annu. Rev. Phys. Chem.*, 2008, **59**, 291-317.
34. N. T. Hunt, *Chem. Soc. Rev.*, 2009, **38**, 1837-1848.
35. J. Zheng, K. Kwak and M. D. Fayer, *Acc. Chem. Res.*, 2006, **40**, 75-83.
36. M. Khalil, N. Demirdöven and A. Tokmakoff, *J. Phys. Chem. A*, 2003, **107**, 5258-5279.
37. C. R. Baiz, P. L. McRobbie, J. M. Anna, E. Geva and K. J. Kubarych, *Acc. Chem. Res.*, 2009, **42**, 1395-1404.
38. S. Park and M. Ji, *ChemPhysChem*, 2011, **12**, 799-805.
39. L. J. G. W. van Wilderen, A. T. Messmer and J. Bredenbeck, *Angew. Chem. Int. Ed.*, 2014, **53**, 2667-2672.
40. C.-h. Tseng, S. Matsika and T. C. Weinacht, *Opt. Express*, 2009, **17**, 18788-18793.
41. U. Selig, C.-F. Schleussner, M. Foerster, F. Langhojer, P. Nuernberger and T. Brixner, *Opt. Lett.*, 2010, **35**, 4178-4180.
42. G. Auböck, C. Consani, F. van Mourik and M. Chergui, *Opt. Lett.*, 2012, **37**, 2337-2339.
43. B. A. West and A. M. Moran, *J. Phys. Chem. Lett.*, 2012, **3**, 2575-2581.
44. N. Krebs, I. Pugliesi, J. Hauer and E. Riedle, *New J. Phys.*, 2013, **15**, 085016.
45. P. Nuernberger, G. Vogt, G. Gerber, R. Improta and F. Santoro, *J. Chem. Phys.*, 2006, **125**, 044512.
46. S. Schott, A. Steinbacher, J. Buback, P. Nuernberger and T. Brixner, *J. Phys. B: At., Mol. Opt. Phys.*, 2014, **47**, 124014.
47. K. Wynne, G. D. Reid and R. M. Hochstrasser, *J. Chem. Phys.*, 1996, **105**, 2287-2297.
48. I. H. M. van Stokkum, D. S. Larsen and R. van Grondelle, *Biochim. Biophys. Acta, Bioenerg.*, 2004, **1657**, 82-104.
49. K. M. Mullen and I. H. M. van Stokkum, *J. Stat. Software*, 2007, **18**, 1-46.
50. J. J. Snellenburg, S. Laptenok, R. Seger, K. M. Mullen and I. H. M. van Stokkum, *J. Stat. Software*, 2012, **49**, 1-23.